High pressure phase equilibrium of ternary and multicomponent alkane mixtures in the temperature range from (283–473) K

Regueira Muñiz, Teresa; Liu, Yiqun; Wibowo, Ahmad A.; Ashrafi, Mehrshad; Varzandeh, Farhad; Pantelide, Georgia; Stenby, Erling Halfdan; Yan, Wei

Published in:
Fluid Phase Equilibria

Link to article, DOI:
10.1016/j.fluid.2017.06.021

Publication date:
2017

Document Version
Peer reviewed version

Accepted Manuscript

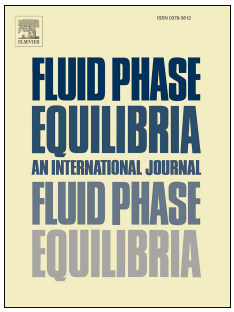

High pressure phase equilibrium of ternary and multicomponent alkane mixtures in the temperature range from (283–473) K

Teresa Regueira, Yiqun Liu, Ahmad A. Wibowo, Mehrshad Ashrafi, Farhad Varzandeh, Georgia Pantelide, Erling H. Stenby, Wei Yan

PII: S0378-3812(17)30253-4

DOI: 10.1016/j.fluid.2017.06.021

Reference: FLUID 11516

To appear in: *Fluid Phase Equilibria*

Received Date: 4 May 2017

Revised Date: 10 June 2017

Accepted Date: 22 June 2017

Please cite this article as: T. Regueira, Y. Liu, A.A. Wibowo, M. Ashrafi, F. Varzandeh, G. Pantelide, E.H. Stenby, W. Yan, High pressure phase equilibrium of ternary and multicomponent alkane mixtures in the temperature range from (283–473) K, *Fluid Phase Equilibria* (2017), doi: 10.1016/j.fluid.2017.06.021.

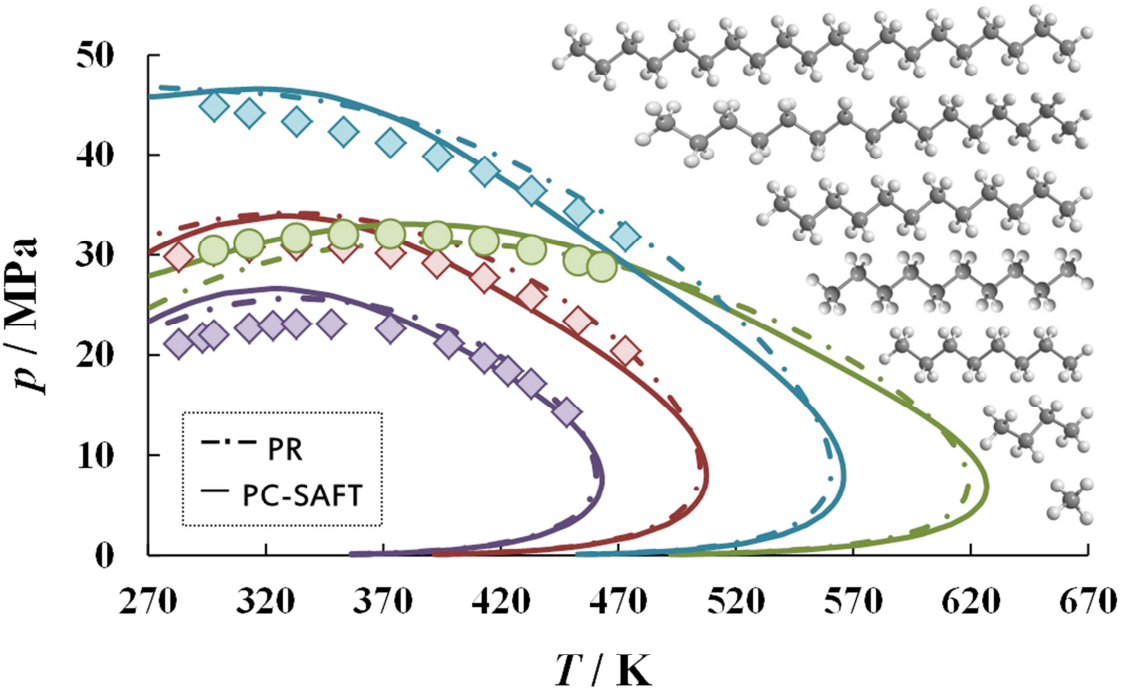

High pressure phase equilibrium of ternary and multicomponent alkane mixtures in the temperature range from (283 to 473) K

Teresa Regueira, Yiqun Liu, Ahmad A. Wibowo, Mehrshad Ashrafi, Farhad Varzandeh, Georgia Pantelide, Erling H. Stenby, Wei Yan*

Center for Energy Resources Engineering (CERE), Department of Chemistry, Technical University of Denmark, DK-2800 Kgs. Lyngby, Denmark

*Corresponding author: E-mail: weya@kemi.dtu.dk; Tel.:+45 45252379

ABSTRACT

Asymmetric multicomponent alkane mixtures can be used as model systems for reservoir fluids. We have prepared two ternary mixtures, methane/n-butane/n-decane and methane/n-butane/n-dodecane, and two multicomponent mixtures composed of methane/n-butane/n-octane/n-dodecane/n-hexadecane/n-eicosane as model reservoir fluids and measured their phase equilibrium in the temperature range from (283 to 473) K by using a variable volume cell with full visibility. Their phase envelopes and liquid volume fractions below the saturation pressure have been measured. Four equations of state, including Soave-Redlich-Kwong (SRK), Peng-Robinson (PR), Perturbed Chain Statistical Associating Fluid Theory (PC-SAFT), and Soave-Benedict-Webb-Rubin (Soave-BWR), have been used to predict phase equilibrium of the measured systems. PR and PC-SAFT give better results than others and Soave-BWR gives poor phase envelope predictions which are quite distinct from the predictions by other models. It is generally challenging for any of the tested models to predict all the measured phase envelopes with high accuracy. For predictive calculation of the liquid fractions, the agreement in the low pressure region is good whereas the fractions just below the saturation pressures are difficult to predict. Moreover GERG-2008 has also been tested with the measured methane/n-butane/n-decane system. It over predicts the saturation pressures but predicts low pressure liquid fractions quite accurately.

Keywords: n-alkanes mixture, phase equilibrium, liquid fraction, high pressure, high temperature

1. INTRODUCTION

Due to the declining conventional oil and gas resources, oil companies tend to explore and produce from more difficult resources such as tight formations, heavy oil, and deeper reservoirs often at high pressure and high temperature (HPHT) conditions [1,2]. For offshore HPHT fields [3], the exploration and production becomes even more costly and risky, requiring a more accurate description of the production and a more careful design. In order to design and forecast the production of these HPHT reservoirs, an accurate description of the relevant phase equilibrium and

fluid properties is one of the prerequisites. However, experimental data for reservoir fluids are usually scarce and it is also challenging to model the phase behaviour of these systems.
The phase equilibrium data of multicomponent n-alkane systems is important to many industrial applications, such as coal liquefaction, oil refining, gas processing or enhanced oil recovery [4]. These multicomponent systems are particularly useful to development of relevant models in the upstream of the oil industry due to their similarity to reservoir fluids. Actually, as the reservoir fluid samples are expensive to acquire and not easily available, an alternative approach is to use well-defined hydrocarbon mixtures as model reservoir fluids. This allows the investigation on the contribution of the main compounds of reservoir fluids to the phase behaviour if the model fluids can capture the main features of the reservoir fluids from the well [5,6]. New experimental data are useful to evaluate predictive thermodynamic models [7-11]. The performance of these models for alkane mixtures can somewhat reflect their performance for real oil and gas systems [5]. Another advantage of using the hydrocarbon mixtures is that reservoir fluid characterization is avoided and the uncertainty of the ill-defined heptane plus fractions in the reservoir fluids will not affect the modelling results.

The objective of this work is to measure new data of phase equilibrium for ternary and multicomponent alkane mixtures as model reservoir fluids. The data for these mixtures under high pressure conditions are far from systematic, especially for highly asymmetric ones. Among others, it is worth mentioning several previous works which studied vapour-liquid phase equilibria of ternary alkane mixtures, such as Urlic et al. [12] who reported values of phase equilibrium data of the ternary system methane/n-butane/n-decane, also Reamer et al. [13-17] studied the ternary systems methane/n-butane/n-decane and methane/n-propane/n-decane and Kariznovi et al. [18,19] reported vapour-liquid equilibrium data of the methane/n-decane/n-tetradecane and methane/n-decane/n-hexadecane systems. Moreover Cebola et al. [20] studied the phase behaviour of the ternary mixture methane/n-hexane/n-tetradecane, Gregorowicz et al. [21] determined liquid-liquid-vapour equilibrium of the ternary system methane/n-propane/n-eicosane and Machado and de Loos [22] determined phase equilibrium data on the ternary system methane/tetracosane/triacontane. Other studies of ternary mixtures include those of Yang et al. [23] for the system methane/n-butane/n-octane, Uribe-Vargas and Trejo [24] for the system methane/n-hexane/n-decane and Blanco et al. [25] who determined dew points of the ternary system methane/ethane/butane. As concerns the study of phase equilibria of multicomponent alkane mixtures, previous results have been published by Daridon et al. [26] reporting phase behaviour of multicomponent mixtures composed of methane/n-decane/heavy fraction, the heavy fraction contained n-alkanes ranging from n-octadecane to n-triacontane, Gonzalpour et al. [27] analysed the vapour-liquid equilibrium of a 5-component synthetic gas condensate containing methane/n-propane/n-pentane/n-decane/n-hexadecane, Mørch et al. [28] determined dew points of five synthetic natural gas (SNG) mixtures containing ethane/propane/i-butane/n-butane/n-pentane, Nourozieh et al. [29] reported vapour-liquid equilibrium data of the ternary system methane/n-decane/n-octadecane, Pauly et al. [30,31] measured the phase equilibrium data of multicomponent systems composed of methane plus a heavy fraction which ranged from n-tridecane to n-docosane, Shariati et al. [5,32] determined bubble-point pressures of 5-component model gas condensate systems and also of synthetic

mixtures containing methane plus a heavy fraction C_6^+ which included alkanes, cycloalkanes, and aromatics, whereas Fenghour et al. [33] determined bubble points of the multicomponent mixture composed of methane/n-butane/n-heptane/n-hexadecane.

In our previous work [34] we investigated the phase behaviour of binary hydrocarbon mixtures composed of methane and n-decane. As a continuation, we measured in the present work the saturation pressures of two ternary and two 6-component alkane mixtures and their liquid fractions in the two-phase region. The studied systems can serve as model systems for real volatile oil and gas condensate fluids. Specifically the two ternary mixtures include one mixture of methane/n-butane/n-decane studied in the temperature range from (283 to 448) K and another mixture of methane/n-butane/n-dodecane studied in the temperature range from (283 to 473) K. The two 6-component mixtures are made up of methane/n-butane/n-octane/n-dodecane/n-hexadecane/n-eicosane with compositions representative for a low gas oil ratio (GOR) fluid and a high GOR fluid. The 6-component mixtures were studied in the temperature range from (298 to 473) K. Several equations of state (EoS), including Soave-Redlich-Kwong [35], Peng-Robinson [36], Perturbed Chain Statistical Associating Fluid Theory [37], Soave-Benedict-Webb-Rubin [38], and GERG-2008 [39], were selected to model the measured phase equilibrium. The binary interaction parameters for all these models are optimized values taken from the literature [40] in order to test the predictive capability of these models. GERG-2008 was only applied to the methane/n-butane/n-decane system because the current GERG-2008 does not have parameters for the other heavier n-alkanes.

2. MATERIALS AND METHODS

2.1. Materials and preparation of sample mixtures

The chemicals used in the present work were methane, n-butane, n-octane, n-decane, n-dodecane, n-hexadecane and n-eicosane. Their provider and purity are indicated in Table 1. N-octane, n-decane, n-dodecane and n-hexadecane were degassed by using an ultrasonic bath Branson 1510 DTH for at least 1800 s prior to their use.

Table 1. Provider and mole fraction purity of the chemicals

Chemical name	Provider	Purity*
methane	AGA gas	0.999995
n-butane	AGA gas	0.9995
n-octane	Sigma-Aldrich	0.994[a]
n-decane	Sigma-Aldrich	0.998[a]
n-dodecane	Sigma-Aldrich	0.993[a]
n-hexadecane	Sigma-Aldrich	0.994[a]
n-eicosane	Sigma-Aldrich	0.996[a]

*Given by the manufacturer

[a]Gas chromatography

In this work we prepared two ternary mixtures composed of methane/n-butane/n-decane and of methane/n-butane/n-dodecane. Moreover we prepared two 6-component mixtures composed of methane/n-butane/n-octane/n-dodecane/n-hexadecane/n-eicosane. These mixtures were prepared by using a high pressure cylinder with a piston inside. The piston separates the prepared sample mixture from the hydraulic fluid (water) used for pressurization. There is a stainless-steel ball on the sample side of the high pressure cylinder to homogenize the sample.

In the preparation of a sample mixture, the sample side of the high pressure cylinder was first evacuated by using a vacuum pump Edwards E2M1.5 for at least 3600 s. The liquid compounds of the mixture were then added to the sample side of the high pressure cylinder through a burette with a standard uncertainty of 0.01 cm^3. In the case of the ternary mixtures a known volume of n-decane or n-dodecade was added by using the burette. As concerns the multicomponent mixtures, first a liquid mixture containing n-octane/n-dodecane/n-hexadecane/n-eicosane was prepared gravimetrically using an analytical balance Mettler-Toledo PR 1203 which has a standard uncertainty of 0.001 g and then this mixture was loaded into the evacuated sample cylinder with the aforementioned burette. Density values of n-decane, n-dodecane and the liquid mixture (n-octane/n-dodecane/n-hexadecane/n-eicosane) were used to obtain the mass of liquid added to the high pressure cylinder. Densities of n-decane and n-dodecane were taken from the NIST Standard Reference Database 23, Version 9.1 [41], which uses the values from Lemmon and Span [42] for n-decane and those from Lemmon and Huber [43] for n-dodecane. As concerns the density of the liquid mixtures of n-octane/n-dodecane/n-hexadecane/n-eicosane at ambient temperature, they were measured through a densimeter Anton Paar DMA 4100, which has a standard density uncertainty of 0.0001 $g \cdot cm^{-3}$. The measured densities are presented in Table 2.

Table 2. Densities of the liquid mixtures composed of n-octane/n-dodecane/n-hexadecane/n-eicosane at ambient pressure.

T^*/K	$x_{\text{n-octane}}$	$x_{\text{n-dodecane}}$	$x_{\text{n-hexadecane}}$	$x_{\text{n-eicosane}}$	$\rho^{\S}$/ $g \cdot cm^{-3}$
295.85	0.4229	0.2941	0.2123	0.0707	0.7448
295.95	0.3889	0.2772	0.1675	0.1664	0.7505

*Temperature standard uncertainty $u(T)$=0.02 K

§Density standard uncertainty $u(\rho)$=0.0001 $g \cdot cm^{-3}$

After the liquids were loaded in the high pressure cylinder, n-butane was added gravimetrically, followed by methane by using the aforementioned analytical balance. Once all the compounds of the mixture were added to the high pressure cylinder, the pressure of the prepared sample was increased using a syringe pump (Teledyne Isco 100 DX) to a value at least 3 MPa above the estimated saturation pressure. The cylinder was rocked to ensure that a homogeneous single-phase mixture was prepared. The final composition of the ternary and multicomponent mixtures studied in this work is presented in Table 3. The uncertainty of the mole fraction composition with an expanded uncertainty k=2 is $6 \cdot 10^{-4}$.

Table 3. Composition in mole fraction[a] of the ternary (C_1-C_4-C_{10} and C_1-C_4-C_{12}) and multicomponent (low GOR and high GOR) mixtures studied in this work.

Compound	C_1-C_4-C_{10}	C_1-C_4-C_{12}	Low GOR	High GOR
methane	0.8119	0.8512	0.7000	0.8997
n-butane	0.1385	0.0991	0.1200	0.0300
n-octane	–	–	0.0700	0.0297
n-decane	0.0496	–	–	–
n-dodecane	–	0.0497	0.0499	0.0207
n-hexadecane	–	–	0.0301	0.0149
n-eicosane	–	–	0.0300	0.0050

[a]Expanded mole fraction uncertainty $U(x)$ (k=2): $6 \cdot 10^{-4}$

2.2. Experimental set-up

The schematic of the high pressure PVT apparatus is given in Figure 1. The main component of this apparatus is a PVT cell PVT 240/1500 FV (full visibility) from Sanchez Technologies. The cell is a stainless steel cylinder with a motor driven piston at one end to vary the cell volume precisely. It has a maximum volume of 240 cm^3 and can operate up to 473.15 K and 150 MPa. There is a sapphire window at the other end of the cell which allows visual observation of all the space inside the cell. A CCD digital camera Lumenera Lw1335C is installed in front of the window for remote monitoring. The sample inside the cell can be agitated by means of a mechanical stirrer attached to the head of the piston. The stirrer has four retractable blades to reduce the dead volume of the PVT cell. The whole apparatus is controlled by computer through the Falcon Software.

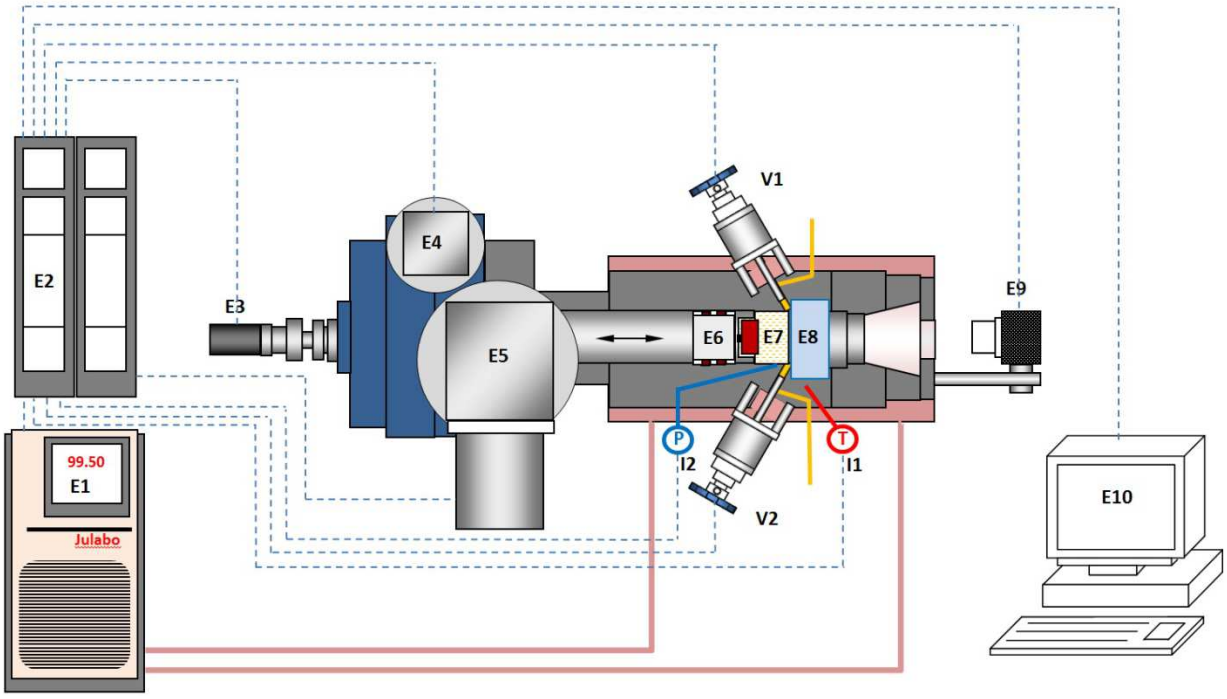

Figure 1. Scheme of the PVT apparatus. (E1) thermostatic bath, (E2) control box, (E3) stirrer motor, (E4) piston motor, (E5) rotation system, (E6) piston with retractable blades, (E7) cell, (E8) sapphire window, (E9) video camera, (E10) computer, (I1) Pt100, (I2) pressure transducer, (V1,V2) high pressure valves.

The temperature of the PVT cell is measured through a Pt100 located in the wall of the cell within 0.02 K. The Pt100 uses the resistance of a platinum element to measure temperature. It has a resistance of 100Ω at 0°C and the relationship between temperature and resistance is relatively linear. The temperature sensor is located in the wall of the PVT cell and the temperature is read in the Falcon Software which controls the PVT apparatus. The temperature control is performed through an electric heating system comprised of eight heating resistances, moreover the stability of the temperature is improved by means of a circulating bath Julabo Presto A40 connected to a jacket covering the cell, which can also be used to cool down the system.

The system pressure is measured by a pressure transducer Dynisco PT435A which incorporates a 350 Ω bonded foil strain gage Wheatstone Bridge. This technology provides an output of 0 - 3.33 mV/V (nominal), proportional to pressure. It has originally been calibrated by Dynisco through a calibration apparatus traceable to NIST and it is calibrated against a reference pressure gauge SIKA type P (0.05% FS) prior to the measurement of a new system in the PVT apparatus. The readings of this pressure transducer are displayed in the Falcon Software. The pressure calibration is performed as a function of temperature in the experimental pressure range against a reference pressure transducer which leads to a pressure standard uncertainty of 0.06 MPa in the present work.

2.3. Experimental procedure

The determination of the saturation pressure by visual observation was performed in triplicate through pressure reduction at constant flow rate ($1.4 \cdot 10^{-4}$ $cm^3 s^{-1}$) from the single phase until the appearance of a new phase. The appearance of a new phase can be observed as a bubble (bubble point), as a drop (dew point) or as a cloud (bubble or dew point). The appearance of the cloud is observed when the density of the incipient phase is similar to that of the original phase, which occurs in pressure and temperature conditions close to the critical point. It is estimated that the combined standard uncertainty of the equilibrium pressure determined through the visual observation is 0.10 MPa for bubble and dew points and 0.15 MPa for cloud points.

The liquid fractions upon expansion below the saturation pressure were determined in a constant mass expansion (CME) process programed in the Falcon software. The CME process consists of expansions of the same sample mixture to a series of pressure stages below the saturation pressure. In our experiment, this was achieved by a series of expansion steps to pre-defined volumes. When a pre-defined volume was reached, a stirring time of at least 60 s was applied followed by subsequent waiting times of 300 s until the pressure was stable within 0.05 MPa. Once the stability is achieved, a photo of the mixture in the cell was taken by the Euclide software. Liquid and gas volumes were measured from each photo, based on geometric relations, by means of this software. The user needs to set the level of the observed gas-liquid interface by means of this software and the calculation of the liquid and gas volumes is automatically performed by the software taking into account the total

volume of the system and the geometrical dimensions of the cell. The maximum standard uncertainty of the liquid fractions reported in this work is 0.013. The liquid fraction measurement was also used to judge the phase transition type when the measured saturation point was a cloud point. An increase in the liquid fraction with expansion right below the saturation pressure indicated a dew point phase transition, whereas a decrease in the liquid fraction right below the saturation pressure indicated a bubble point phase transition.

The above experimental procedure was applied to determine the saturation pressures for the n-alkane mixtures presented in Table 3 in the temperature range from (283 to 448) K for the C_1-C_4-C_{10} system, from (283 to 473) K for the C_1-C_4-C_{12} system, from (298 to 473) K for the low and high GOR systems, and to measure the liquid fractions in the two-phase regions of these systems in the same temperature ranges.

2.4. Modelling

Two classical cubic EoSs (SRK [35] and PR [36]) and three non-cubic EoSs (PC-SAFT [37], Soave-BWR [38], and GERG-2008 [39]) were used here to model the phase envelopes and liquid fractions of the studied multicomponent systems. We present below only a brief description of the non-cubic models.

PC-SAFT EoS

The PC-SAFT EoS was proposed by Gross and Sadowski [37] to model asymmetric and highly non-ideal systems and has the following form in terms of the reduced Helmholtz energy $\tilde{a}$:

$$\tilde{a} = \tilde{a}^{id} + \tilde{a}^{hc} + \tilde{a}^{disp} + \tilde{a}^{assoc} \quad (1)$$

In this equation, $\tilde{a}^{id}$ is the ideal gas contribution, $\tilde{a}^{hc}$ is the contribution of the hard-sphere chain reference system, $\tilde{a}^{disp}$ is the dispersion contribution arising from the square well attractive potential and $\tilde{a}^{assoc}$ is the association contribution based on Wertheim's theory [37].

For hydrocarbon systems consisting only of non-associating components, the $\tilde{a}^{assoc}$ term in eq 1 is zero because there is no association in these systems. There are only three model parameters for a non-associating component, the chain length *m*, the segment diameter σ and the segment energy ε.

von Solms et al. [44] simplified the original PC-SAFT EoS by assuming that all the segments in the mixture have the same mean diameter *d*, which gives a mixture volume fraction identical to that of the actual mixture. The simplified version of PC-SAFT is used in our discussion here.

Soave-BWR EoS

The Soave-BWR EoS refers to a recent modification of the Benedict-Webb-Rubin (BWR) EoS [45] given by Soave [38]:

$$Z = \frac{P}{RT\rho} = 1 + B\rho + D\rho^4 + E\rho^2(1 + F\rho^2)\exp(-F\rho^2) \quad (2)$$

where Z is the compressibility factor, ρ is the density, and B, D, E, and F are the model coefficients which are functions of three model parameters for each component, T_c, P_c, and ω. Further details about Soave-BWR EoS can be found elsewhere [38].

GERG-2008 EoS

GERG-2008 is based on a multi-fluid mixture model and is a wide-range EoS developed for 21 components of natural gases and their mixtures. It is valid over the temperature range from (60 to 700) K and up to 70 MPa [39]. The dimensionless form of the reduced Helmholtz free energy given by this EoS is as follows:

$$\alpha(\delta,\tau,\bar{x}) = \alpha^0(\rho,T,\bar{x}) + \sum_{i=1}^{n} x_i \alpha_{0i}^r(\delta,\tau) + \Delta\alpha^r(\delta,\tau,\bar{x}) \quad (3)$$

where δ is the reduced mixture density, τ is the inverse reduced mixture temperature, $\bar{x}$ is the vector of mole fractions, and $\alpha^0(\rho,T,\bar{x})$ is the dimensionless form of the Helmholtz free energy for the ideal-gas mixture. The last two terms on the right hand side of eq 3 represent the residual part of the reduced Helmholtz free energy of the mixture, where $\sum_{i=1}^{n} x_i \alpha_{0i}^r(\delta,\tau)$ is the residual part of the reduced Helmholtz free energy of component i, and $\Delta\alpha^r(\delta,\tau,\bar{x})$ is the contribution to the reduced residual Helmholtz free energy due to mixing at constant δ and τ.

More information about GERG-2008 can be found in the original article [39]. As this model is developed for n-alkanes up to nC_{10}, it has only been used for calculation of the phase envelope and liquid fraction of the C_1-C_4-C_{10} system in this study. The parameters used in this model for this ternary system were taken from Kunz and Wagner [39].

The pure compound parameters used in the models, as well as the binary interaction parameters are gathered in tables 4 and 5, respectively. Only binary interaction parameters for the methane/n-alkane pairs were used in this work. The interaction parameters between other pairs are usually small and do not influence the calculation results significantly.

Table 4. Pure compound parameters for SRK, PR, PC-SAFT, S-BWR EoSs and GERG-2008.

	methane	n-butane	n-octane	n-decane	n-dodecane	n-hexadecane	n-eicosane
T_c / K[*]	190.56[‡]	425.12[‡]	568.70[‡]	617.70[‡]	658.00[‡]	723.00[‡]	768.00[†]
p_c / MPa[*]	4.599[‡]	3.796[‡]	2.490[‡]	2.110[‡]	1.820[‡]	1.400[‡]	1.160[†]
ω[*]	0.0115	0.2002	0.3996	0.4923	0.5764	0.7174	0.9069
σ / Å[§]	3.7039	3.7086	3.8373	3.8384	3.8959	3.9552	3.9120
εk^{-1} / K[§]	150.03	222.88	242.78	243.87	249.21	254.70	251.92
m[§]	1.0000	2.3316	3.8176	4.6627	5.3060	6.6485	8.4092

[*]DIPPR database [46]

[§]Gross and Sadowski [37]

[‡]Ambrose and Tsonopoulos [47]

[†]Tsonopoulos and Tan [48]

Table 5. Methane/n-alkane binary interaction parameters, k_{ij}, for SRK, PR, PC-SAFT and S-BWR, taken from Yan et al. [40]

k_{ij}	SRK	PR	PC-SAFT	S-BWR
methane/n-butane	0.0100	0.0168	0.0041	-0.0044
methane/n-octane	0.0410	0.0451	0.0159	-0.0149
methane/n-decane	0.0411	0.0409	0.0172	-0.0311
methane/n-dodecane	0.0442	0.0500	0.0103	-0.0315
methane/n-hexadecane	0.0586	0.0561	0.0189	-0.0441
methane/n-eicosane	0.0534	0.0541	0.0172	-0.0405

3. RESULTS AND DISCUSSION

In this section the quantitative comparison between the obtained experimental data and literature data is performed by using the absolute average deviation (AAD) according to the following equation:

$$AAD/\% = \frac{100}{k}\sum_{i=1}^{k}\left|\frac{Y^{Lit.}-Y^{Exp.}}{Y^{Lit.}}\right| \quad (4)$$

where k is the number of experimental data points, Y stands for the analysed property and *Exp.*, *Lit.*, stand for experimental and literature, respectively.

Also the quantitative analysis of the model performance is given through the absolute average deviation (AAD), in this case obtained by using the following equation:

$$AAD/\% = \frac{100}{k}\sum_{i=1}^{k}\left|\frac{Y^{Calc.}-Y^{Exp.}}{Y^{Exp.}}\right| \quad (5)$$

where k is the number of experimental data points, Y stands for the analysed property and *Cal.*, *Exp.*, stand for calculated and experimental, respectively.

The measured saturation pressures for the two ternary mixtures and the two 6-component mixtures are presented in Table 6. In the studied temperature ranges, maximum saturation pressures of 23.1, 30.9, 32.1 and 44.8 MPa were observed for the C_1-C_4-C_{10}, C_1-C_4-C_{12}, low GOR and high GOR systems, respectively. All the measured bubble and dew point pressures for the mixtures described in Table 3 are also depicted in Figure 2 as a function of temperature. It should be noted that for the mixture C_1-C_4-C_{10} no phase transition was observed at 472.55 K when decreasing the pressure from (25.27 to 6.74) MPa. Additionally, for the low GOR mixture at 472.37 K, it was not easy to detect the phase transition because the formed cloud was weak. Although the saturation pressure was

found to be in the pressure range from (28.0 to 28.3) MPa, no saturation pressure at this temperature was reported in Table 6 due to the large uncertainty.

Urlic et al. [12] reported previously saturation pressures in the temperature range from (254 to 462) K for the methane/n-butane/n-decane system with mole fractions of 0.41, 0.14 and 0.05 for methane, n-butane and n-decane, respectively. These literature values [12] are also depicted in Figure 2 (a). The results obtained in the present work in the temperature range from (283 to 348) K for the C_1-C_4-C_{10} system were compared with the results previously reported by Urlic et al. [12]. A comparison was also made at 448.10 K, where the saturation pressure from this work was compared with the interpolated saturation pressure between 446.95 K and 449.07 K reported by Urlic et al. [12]. The overall comparison yielded an AAD of 1.04%, which indicates a good agreement between the results measured in the present work and those from literature.

Table 6. Saturation pressures of the ternary and multicomponent systems studied in this work.[a]

T/K	*p*/MPa	*T*/K	*p*/MPa	*T*/K	*p*/MPa	*T*/K	*p*/MPa
C_1-C_4-C_{10}[*]		C_1-C_4-C_{12}[*]		Low GOR[§]		High GOR[*]	
283.08	21.1	283.10	29.8	298.08	30.4	298.13	44.8
293.08	21.7	298.06	30.4	313.12	31.1	313.12	44.2
298.08	22.0	313.04	30.7	333.13	31.7	333.18	43.3
313.07	22.6	333.00	30.9	353.12	32.0	353.23	42.3
323.14	22.9	353.04	30.7	373.19	32.1	373.22	41.2
333.13	23.1	373.10	30.1	393.12	31.8	393.34	39.8
348.07	23.1	393.02	29.1	413.14	31.3	413.27	38.3
373.16	22.6	413.01	27.7	433.13	30.5	433.15	36.4
398.02	21.1	432.99	25.8	453.13	29.4	453.16	34.3
413.10	19.6	452.97	23.4	463.17	28.7	473.12	31.8
423.11	18.4	473.15	20.4				
433.10	17.1						
448.10	14.3						

[*]The reported saturation pressures are dew points.

[§]The reported saturation pressures are bubble points.

[a]Standard temperature uncertainty $u(T)$: 0.02 K; Combined standard pressure uncertainty $u(p)$:0.15 MPa

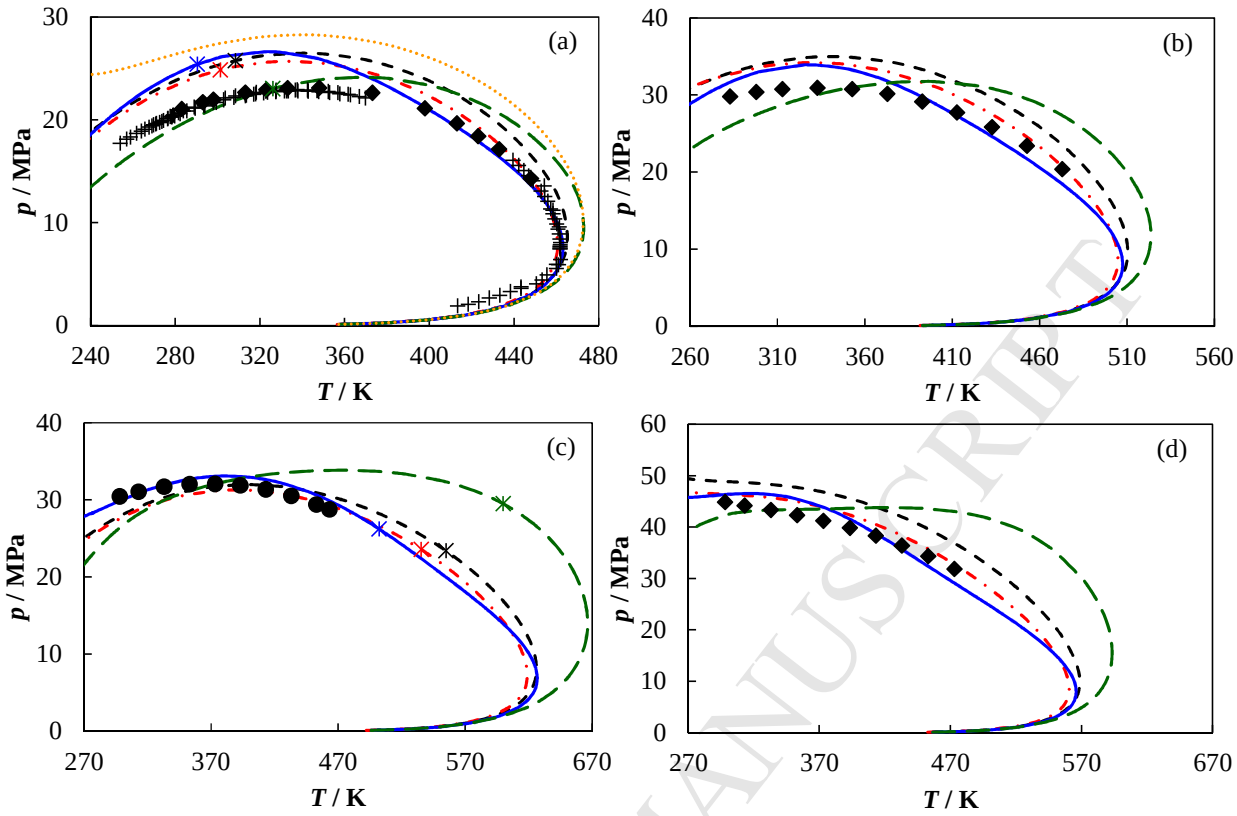

Figure 2. Bubble (●) and dew (◆) point pressures for the systems studied in this work (Table 3). (a) C_1-C_4-C_{10} system, (b) C_1-C_4-C_{12} system, (c) low GOR system and (d) high GOR system. Saturation pressures reported by Urlic et al. [12] for the system C_1-C_4-C_{10} (+). SRK (black dashed line), PR (red dashed-dotted line), PC-SAFT (blue solid line), Soave-BWR (green long-dashed line) and GERG-2008 (orange dotted-line). Critical points predicted by the different models (∗).

Figure 2 illustrates also the phase envelope calculation results for the four mixtures using different EoSs. The binary interaction parameters for SRK, PR, Soave-BWR and PC-SAFT were regressed from binary vapor-liquid equilibrium data [40] (see table 5). Since no adjustment is made here for any specific ternary or multicomponent mixture here, the calculation can be considered as a test for the prediction capability of the EoSs. It can be observed in Figure 2 (a) that for the C_1-C_4-C_{10} mixture PC-SAFT, SRK and PR give more or less accurate prediction of the dew point pressures at temperatures higher than 380 K. However, all the three EoSs, over predict the experimental data at lower temperatures. Soave-BWR seems to give better estimation of the dew point pressures at lower temperatures, but it over predicts the experimental data at higher temperatures. GERG-2008 is the poorest among all EoSs and over predicts the dew point pressures in the whole temperature range. The performance of GERG-2008 in phase envelope calculation of different mixtures of the C_1-C_{10} binary system was previously investigated by Varzandeh et al. [49], where they observed a similar behaviour for GERG-2008, especially at high methane mole fraction. They concluded that Soave-BWR and GERG-2008 were very similar in phase equilibrium calculation and both had challenges in describing highly asymmetric systems, even binary pairs as simple as methane and n-decane.

For the C_1-C_4-C_{12}, the low GOR and the high GOR systems, PC-SAFT and PR give better prediction of the saturation pressures than SRK and Soave-BWR. Soave-BWR gives the poorest results, especially at higher temperatures, and the calculated phase envelopes are larger than those of the other EoSs. PC-SAFT, SRK, and PR give almost accurate prediction of the bubble point pressure for the low GOR system, PC-SAFT being slightly better than SRK and PR. In general, PC-SAFT and PR give more reliable results than the other EoSs for the systems tested.

The predicted saturation pressures of the systems studied in this work are gathered in table A.1 of the supplementary material. Figure 3 summarizes the overall performance of the saturation pressure prediction for all the EoSs. It can be seen that PR and PC-SAFT give the lowest overall deviations in the prediction of the saturation pressures.

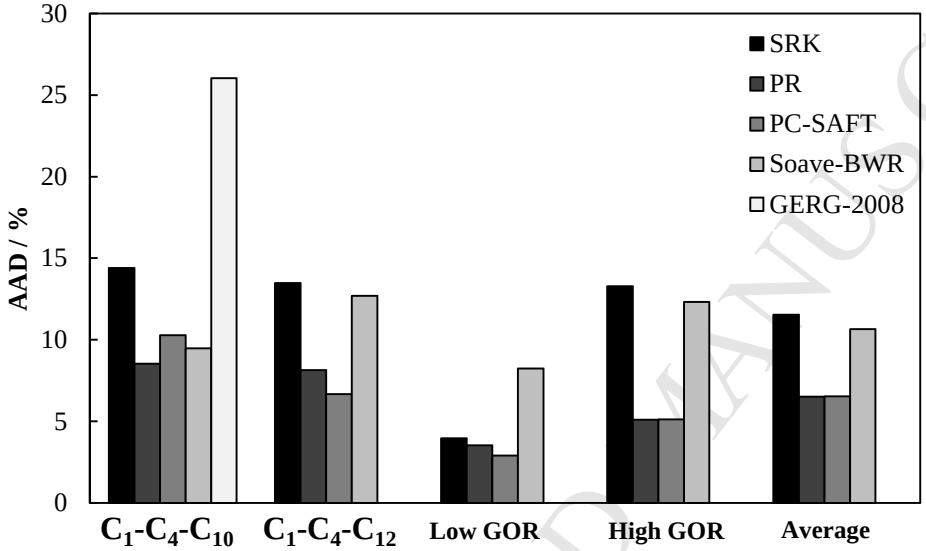

Figure 3. Absolute average deviations (AAD) obtained in the prediction of the saturation pressures by different EoSs.

As concerns the constant mass expansion experiments, the measured liquid fractions below the saturation pressures are summarized in Tables 7 to 10. From the change of the liquid fraction just below the saturation pressure (Tables 7 to 10 and Figure 4), it can be judged that all the measured saturation pressures for the mixtures C_1-C_4-C_{10}, C_1-C_4-C_{12} and the high GOR mixture correspond to dew points, whereas those for the low GOR mixture correspond to bubble points. Figure 4 also illustrates the typical retrograde condensation behavior in the C_1-C_4-C_{10} mixture, the C_1-C_4-C_{12} mixture and the high GOR mixture: starting from a zero liquid fraction at the saturation point, the liquid fraction increases as the pressure decreases just below the saturation pressure up to a maximum, after which a further decrease of the pressure leads to a decrease in the liquid fraction. The maximum liquid fractions obtained under the studied conditions were found at the lowest temperatures for each of the systems, i.e. 283 K for the ternary mixtures C_1-C_4-C_{10} (0.38 liquid fraction) and C_1-C_4-C_{12} (0.31 liquid fraction) and 298 K for the high GOR mixture (0.29 liquid fraction). The measured liquid drop-out for the aforementioned mixtures decreases with temperature and liquid fractions lower than 0.08 were found for these mixtures at the highest studied

temperatures (448 K for the C_1-C_4-C_{10} system and 473 K for the C_1-C_4-C_{12} and high GOR systems). Moreover it can be observed that the slope of the liquid fraction vs. pressure curve just below the saturation pressure decreases as the temperature increases. The large slope found at low temperatures indicates that a small change in pressure results in a large amount of liquid drop-out. As concerns the low GOR mixture, its liquid fraction decreases as the pressure decreases below the saturation point. It can also be observed that close to the bubble point, the slope of the liquid fraction vs. pressure curve is larger at the higher temperatures, which indicates that under these conditions a small pressure change causes vaporization of a large fraction of the mixture into gas. The abrupt change in liquid fraction with pressure is typical for near-critical fluid. For the C_1-C_4-C_{10}, the C_1-C_4-C_{12} and the high GOR mixtures, their critical point temperatures are below the low temperature limit investigated here. The lowest temperatures for these three mixtures are the conditions closest to their critical points and thus correspond to the most dramatic liquid condensation just below their saturation pressures. Similarly, for the high GOR mixture, its critical point is above the high temperature limit investigated here and it is at the highest temperature that this mixture undergoes the dramatic vaporization just below its saturation pressure.

Table 7. Liquid fraction[a] (V_{liquid}/V_{total}) for the system C_1-C_4-C_{10} from Table 3.

p/MPa	Liquid fraction	*p*/MPa	Liquid fraction	*p*/MPa	Liquid fraction	*p*/MPa	Liquid fraction
T = 283.08 K		*T* = 293.21 K		*T* = 298.22 K		*T*= 313.15 K	
20.94	0.363	21.72	0.269	21.90	0.296	22.63	0.175
19.98	0.384	21.61	0.304	21.65	0.314	22.40	0.228
18.39	0.371	21.34	0.337	21.16	0.332	21.95	0.268
15.65	0.305	20.82	0.359	20.23	0.325	21.10	0.277
12.60	0.228	19.88	0.352	18.34	0.297	19.28	0.273
9.42	0.145	17.95	0.323	15.70	0.257	16.64	0.235
6.95	0.096	15.34	0.270	12.56	0.196	13.35	0.180
5.20	0.062	12.26	0.203	10.60	0.154	11.28	0.142
		10.35	0.162	8.17	0.112	8.70	0.102
		7.98	0.113				
T= 348.09 K		*T*= 373.13 K		*T*= 398.01 K		*T*= 413.06 K	
22.82	0.120	22.39	0.047	20.64	0.024	19.44	0.016
22.13	0.168	22.18	0.070	20.24	0.040	19.23	0.024
20.58	0.190	21.97	0.082	19.83	0.052	19.03	0.028
18.13	0.179	21.78	0.092	19.43	0.061	18.83	0.034
14.80	0.143	21.58	0.101	19.03	0.066	18.63	0.039
12.60	0.121	21.36	0.105			18.43	0.043
9.80	0.085					18.13	0.047
T= 423.14 K		*T*= 433.07 K		*T*= 448.13 K			
18.32	0.011	17.01	0.007	14.18	0.004		
18.03	0.019	16.71	0.012	14.08	0.005		
17.72	0.027	16.40	0.018	13.98	0.005		

17.22	0.035	16.20	0.020	13.88	0.006
16.81	0.040	16.00	0.023	13.78	0.006
16.41	0.043	15.80	0.025	13.68	0.007
16.21	0.045	15.70	0.026	13.58	0.007

[a]Standard temperature uncertainty $u(T)$: 0.02 K; Standard pressure uncertainty $u(p)$: 0.06 MPa; Maximum standard liquid fraction uncertainty u(Liquid fraction): 0.013.

Table 8. Liquid fraction[a] (V_{liquid}/V_{total}) for the system C_1-C_4-C_{12} from Table 3.

p/MPa	Liquid fraction	*p*/MPa	Liquid fraction	*p*/MPa	Liquid fraction	*p*/MPa	Liquid fraction
T = 283.01 K		*T* = 298.09 K		*T*= 313.16 K		*T*= 333.10 K	
29.49	0.170	30.11	0.144	30.54	0.101	30.78	0.061
29.07	0.249	29.77	0.219	30.24	0.176	30.53	0.122
28.02	0.294	28.92	0.269	29.50	0.236	29.91	0.182
26.18	0.307	27.29	0.288	28.10	0.265	28.72	0.224
23.22	0.305	24.63	0.282	25.69	0.267	26.65	0.234
18.62	0.267	20.04	0.249	21.48	0.240	22.71	0.209
14.28	0.209	15.56	0.194	16.68	0.188	17.93	0.167
10.41	0.150	11.27	0.141	12.07	0.132	13.04	0.121
7.59	0.101	8.18	0.095	8.74	0.091	9.45	0.085
5.61	0.070	6.04	0.066	6.45	0.062	6.97	0.058
T= 353.15 K		*T*= 373.05 K		*T*= 393.07 K		*T*= 412.98 K	
30.59	0.038	30.02	0.018	29.05	0.008	27.64	0.002
30.39	0.081	29.84	0.049	28.89	0.028	27.50	0.014
29.85	0.137	29.41	0.091	28.54	0.059	27.21	0.033
28.89	0.179	28.57	0.135	27.83	0.096	26.63	0.059
27.07	0.200	27.03	0.162	26.52	0.121	25.52	0.087
23.52	0.190	23.86	0.164	23.75	0.136	23.15	0.108
18.88	0.155	19.48	0.142	19.73	0.125	19.58	0.105
13.85	0.114	14.48	0.106	14.92	0.097	15.07	0.086
10.08	0.078	10.60	0.073	11.03	0.070	11.28	0.062
7.44	0.056	7.86	0.052	8.22	0.049	8.47	0.045
T= 432.96 K		*T*= 452.96 K		*T*= 472.88 K			
25.65	0.006	23.29	0.003	20.29	0.002		
25.40	0.018	23.10	0.005	20.15	0.003		
24.95	0.035	22.74	0.015	19.90	0.006		
24.06	0.055	22.05	0.030	19.41	0.012		
22.10	0.077	20.51	0.048	18.28	0.023		
19.03	0.079	17.98	0.054	16.38	0.031		
14.96	0.070	14.50	0.053	13.58	0.033		
11.38	0.053	11.26	0.042	10.82	0.029		
8.65	0.041	8.68	0.033	8.52	0.023		
		7.06	0.026				

[a]Standard temperature uncertainty $u(T)$: 0.02 K; Standard pressure uncertainty $u(p)$: 0.06 MPa; Maximum standard liquid fraction uncertainty u(Liquid fraction): 0.013.

Table 9. Liquid fraction[a] (V_{liquid}/V_{total}) for the low GOR system from Table 3.

p/MPa	Liquid fraction	p/MPa	Liquid fraction	p/MPa	Liquid fraction	p/MPa	Liquid fraction
T = 298.08 K		T = 313.12 K		T= 333.123 K		T= 353.12 K	
30.16	0.987	30.88	0.995	31.41	0.985	31.91	0.996
29.48	0.955	30.32	0.960	30.93	0.956	31.46	0.956
27.93	0.895	28.96	0.900	29.76	0.898	30.44	0.896
25.34	0.822	26.56	0.821	27.73	0.815	28.66	0.816
21.74	0.734	23.13	0.734	24.54	0.724	25.75	0.719
16.88	0.613	18.16	0.607	19.59	0.606	20.85	0.598
12.45	0.487	13.41	0.486	14.56	0.477	15.62	0.470
8.58	0.355	9.21	0.354	10.00	0.348	10.77	0.345
T= 373.06 K		T= 393.11 K		T= 413.24 K		T= 433.11 K	
31.96	0.988	31.81	0.999	31.29	0.988	30.48	0.983
31.60	0.951	31.54	0.958	31.17	0.965	30.38	0.953
30.71	0.888	30.77	0.885	30.87	0.921	30.15	0.907
29.16	0.808	29.37	0.792	30.28	0.856	29.62	0.831
26.49	0.706	26.97	0.698	29.07	0.769	28.60	0.745
21.82	0.584	22.53	0.576	26.95	0.675	26.73	0.648
16.53	0.463	17.30	0.458	22.89	0.554	23.06	0.536
11.47	0.340	12.10	0.343	17.84	0.442	18.24	0.428
				12.65	0.326	13.09	0.319
T= 453.13 K		T= 463.17 K		T= 473.26 K			
28.90	0.832	28.46	0.766	27.44	0.719		
28.02	0.722	27.65	0.710	26.72	0.639		
26.38	0.622	26.14	0.603	25.35	0.562		
23.06	0.512	22.99	0.496	22.50	0.476		
18.54	0.409	18.64	0.396	18.44	0.381		
13.50	0.306	13.68	0.297	13.69	0.284		

[a]Standard temperature uncertainty $u(T)$: 0.02 K; Standard pressure uncertainty $u(p)$: 0.06 MPa; Maximum standard liquid fraction uncertainty u(Liquid fraction): 0.013.

Table 10. Liquid fraction[a] (V_{liquid}/V_{total}) for the high GOR system from Table 3.

p/MPa	Liquid fraction	p/MPa	Liquid fraction	p/MPa	Liquid fraction	p/MPa	Liquid fraction
T = 298.21 K		T = 313.17 K		T= 333.12 K		T= 353.29 K	
44.72	0.056	44.01	0.034	42.76	0.095	41.94	0.060
44.36	0.140	43.41	0.150	41.69	0.187	41.01	0.151
43.65	0.208	41.99	0.228	39.56	0.237	39.26	0.207
41.94	0.259	39.41	0.263	35.94	0.251	36.19	0.227
38.97	0.285	35.09	0.273	29.57	0.236	30.51	0.220

34.14	0.285	27.99	0.250	22.46	0.192	23.67	0.187
26.52	0.264	20.78	0.199	15.85	0.140	16.88	0.138
19.39	0.209	14.56	0.143	11.31	0.099	12.07	0.098
13.58	0.152	10.38	0.101	8.26	0.071	8.82	0.070
9.74	0.107	7.60	0.073				
7.16	0.075						
T= 373.22 K		*T*= 393.23 K		*T*= 413.24 K		*T*= 433.16 K	
40.93	0.028	39.51	0.032	38.29	0.013	36.06	0.022
40.63	0.070	39.39	0.048	37.55	0.055	35.63	0.044
39.87	0.128	38.86	0.085	36.54	0.094	34.80	0.072
38.44	0.173	37.66	0.132	34.67	0.133	33.23	0.103
35.87	0.199	35.46	0.167	30.78	0.153	29.94	0.126
30.86	0.199	31.02	0.173	25.30	0.139	25.06	0.124
24.44	0.170	25.04	0.157	18.89	0.110	19.08	0.102
17.68	0.128	18.38	0.121	13.84	0.082	14.17	0.076
12.71	0.093	13.33	0.090	10.26	0.060	10.60	0.056
9.31	0.066	9.81	0.065				
T= 453.19 K		*T*= 473.18 K					
33.82	0.016	31.56	0.004				
33.46	0.030	31.15	0.015				
32.79	0.050	30.61	0.029				
31.52	0.073	29.58	0.049				
28.74	0.100	27.27	0.069				
24.50	0.103	23.65	0.078				
19.03	0.086	18.75	0.071				
14.34	0.068	14.37	0.057				
10.84	0.050	10.98	0.044				

[a]Standard temperature uncertainty $u(T)$: 0.02 K; Standard pressure uncertainty $u(p)$: 0.06 MPa; Maximum standard liquid fraction uncertainty u(Liquid fraction): 0.012.

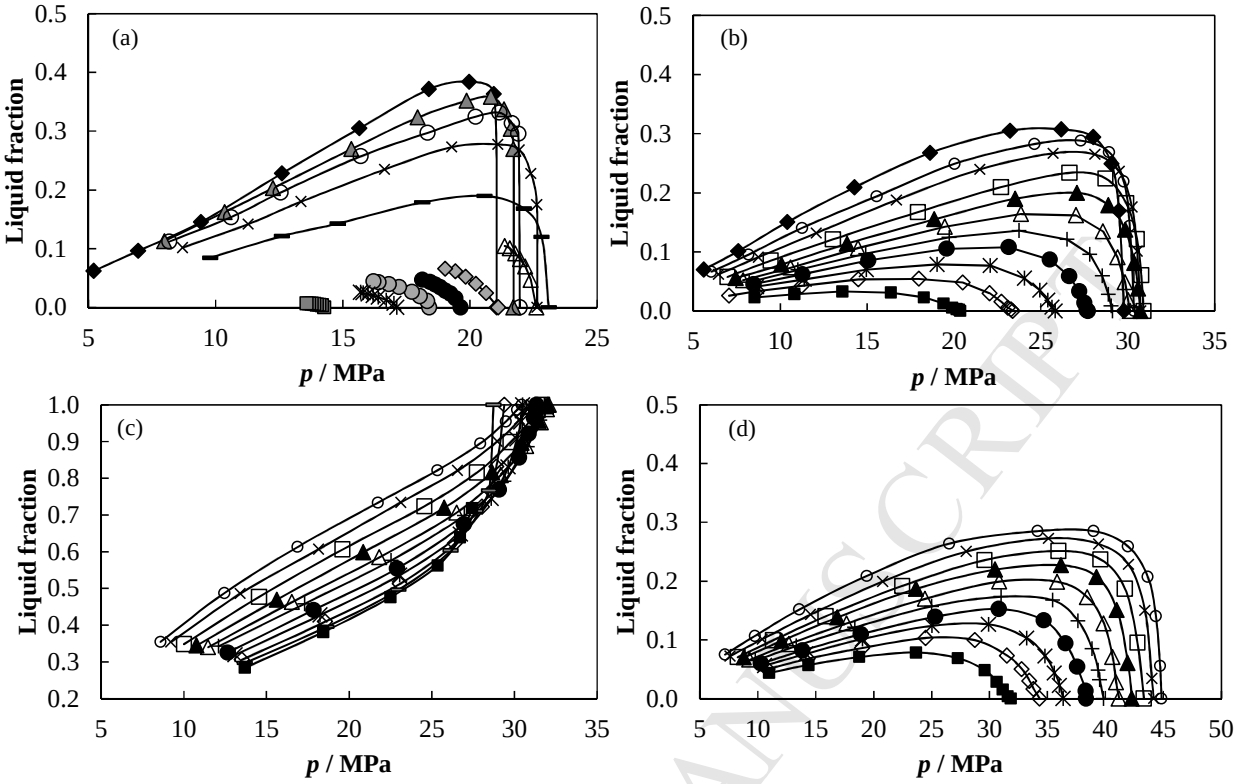

Figure 4. Liquid fraction upon expansion below the saturation pressure for the mixtures presented in Table 3. (a) C_1-C_4-C_{10} mixture, (b) C_1-C_4-C_{12} mixture, (c) low GOR mixture and (d) high GOR mixture. 283 K (◆), 293 K (▲), 298 K (○), 313 K (×), 333 K (□), 348 K (-), 353 K (▲), 373 K (△), 393 K (+), 398 K (◆), 413 K (●), 423 K (●), 433 K (∗), 448 K (■), 453 K (◇), 463 K (-), 473 K (■). The lines are drawn to guide the eyes.

Regarding the liquid fraction prediction, the values obtained by different EoSs at some selected temperatures are depicted in Figure 5. The complete set of predicted liquid fractions at the experimental temperature and pressure conditions through the different models is provided in tables A.2 to A.5 of the supplementary material. In general, all the EoSs have a better performance for the dew point systems in the low pressure range (pressures up to 80 % of the saturation pressure), whereas the prediction is worse at pressures close to the saturation point. It is not surprising if we consider that no fitting of the saturation pressures have been performed. The predicted saturation pressures can have large deviations and some of the saturation point types are even wrongly predicted (Figure 5(a)). The liquid fractions close to the saturation pressures are sensitive to the accuracy of the saturation pressure predictions. For near-critical fluids, the sensitivity is even higher. That is why the deviations close to the saturation pressures are high. As concerns the bubble point system, the prediction of the liquid fraction is acceptable in the whole studied pressure range (AAD lower than 8% for all the models). Since no phase compositions were measured in the two-phase region, the predicted density is influenced by the model performance both in density calculation and composition prediction. Nevertheless, the liquid fraction data reflect how reservoir oil will shrink or how gas condensate will drop out liquid in the two-phase region. The comparison

provides some general insight on how difficult it is to predict the shrinkage/liquid drop-out behavior.

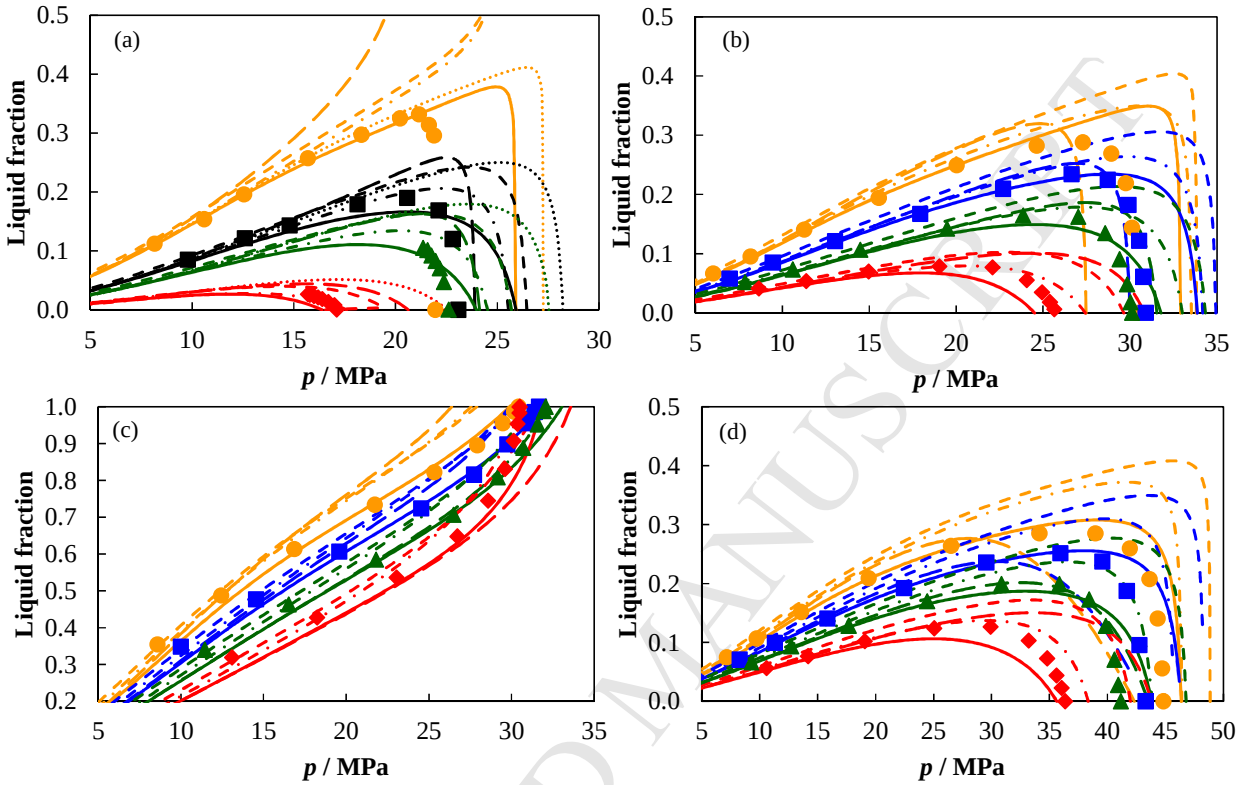

Figure 5. Experimental and calculated liquid fraction upon expansion below the saturation pressure for the mixtures presented in Table 3 at selected temperatures: 298 K (●), 333 K (■), 348 K (■), 373 K (▲) and 433 K (◆). (a) C_1-C_4-C_{10} mixture, (b) C_1-C_4-C_{12} mixture, (c) low GOR mixture and (d) high GOR mixture. SRK (dashed line), PR (dashed-dotted line), PC-SAFT (solid line), Soave-BWR (long-dashed line) and GERG-2008 (dotted-line).

4. CONCLUSIONS

Saturation pressures of four n-alkane mixtures have been accurately determined in the temperature range from (283 to 473 K). Maximum saturation pressures under the studied temperature range of 23.10, 30.91, 32.07 and 44.84 MPa were measured for the C_1-C_4-C_{10}, C_1-C_4-C_{12}, low GOR and high GOR systems, respectively. Under the studied temperature ranges bubble points were found for the low GOR system whereas dew points were found for the C_1-C_4-C_{10}, C_1-C_4-C_{12}, and high GOR systems. For these three dew point mixtures, maximum liquid fractions of 0.38, 0.31 and 0.29 were found for the C_1-C_4-C_{10} system at 283 K, the C_1-C_4-C_{12} at 298 K and the high GOR mixture at 298 K, respectively.

For the three dew point mixtures it has been observed that the slope of the liquid fraction vs. pressure curve just below the saturation pressure decreases as the temperature increases, whereas

for the bubble point mixture (low GOR system) the slope of the liquid fraction vs. pressure curve just below the saturation pressure is higher at the highest temperatures. In general, the liquid fraction-pressure slope is higher as the temperature approaches to the critical temperature. The measured data for these asymmetric systems can serve as useful testing systems for models intended for describing reservoir fluids.

As concerns model performance, PR and PC-SAFT have a better overall performance in the prediction of the experimental saturation pressures. Moreover SRK gives the poorest results for the dew point systems (C_1-C_4-C_{10}, C_1-C_4-C_{12}, and high GOR mixtures), along with GERG-2008 which presents the worst performance for the C_1-C_4-C_{10} system. Concerning the bubble point mixture (low GOR) Soave-BWR gives the worst predictions. Actually, the predictions by Soave-BWR are generally poor and show very different characteristics from the predictions by the other models. In general, it is observed that the model performance is better for the bubble point mixture than for the dew point mixtures, and it is challenging for any of the tested models to predict all the measured phase envelopes with high accuracy. This somehow illustrates the difficulty of predictive modelling of highly asymmetric systems and the necessity of experimental measurement of such systems for model tuning.

Regarding the prediction of the liquid fractions, a good performance for all the models was obtained in the prediction of the low GOR mixture (AAD lower than 8%) whereas for the C_1-C_4-C_{10}, C_1-C_4-C_{12}, and high GOR mixtures the models perform well only in the low pressure range up to around 80 % of the saturation pressure.

ACKNOWLEDGEMENTS

This work has been carried out under the NextOil project sponsored by the Innovation Fund Denmark, DONG E&P and Maersk Oil (Jr. nr. 113-2012-1).

REFERENCES

[1] A. Shadravan, M. Amani, HPHT 101-What petroleum engineers and geoscientists should know about high pressure high temperature wells environment, Energy Sci. Technol., 4 (2012) 36-60.

[2] R.A. Larson, L.L. Duhon, S.P. Benavides, Optimizing wireline formation evaluation in HP/HT wells, Society of Petroleum Engineers, SPE-97569-MS, (2005).

[3] G. Olsvik, S. Howard, J. Downs, The long-term production performance of deep HPHT gas condensate fields developed using formate brines, Society of Petroleum Engineers, SPE-165151-MS, (2013).

[4] K. Nasrifar, N. Rahmanian, High-pressure solubility of light gases in heavy n-alkanes from a predictive equation of state: Incorporating Henry's law constant into binary interaction parameter, Fluid Phase Equilib., 381 (2014) 95-101.

[5] A. Shariati, E.J.M. Straver, L.J. Florusse, C.J. Peters, Experimental phase behavior study of a five-component model gas condensate, Fluid Phase Equilib., 362 (2014) 147-150.

[6] P. Ungerer, B. Faissat, C. Leibovici, H. Zhou, E. Behar, G. Moracchini, J.P. Courcy, High pressure-high temperature reservoir fluids: investigation of synthetic condensate gases containing a solid hydrocarbon, Fluid Phase Equilib., 111 (1995) 287-311.

[7] S.Z. Al Ghafri, G.C. Maitland, J.P.M. Trusler, Experimental and modeling study of the phase behavior of synthetic crude oil + CO2, Fluid Phase Equilib., 365 (2014) 20-40.

[8] M.O. McLinden, M. Richter, Application of a two-sinker densimeter for phase-equilibrium measurements: A new technique for the detection of dew points and measurements on the (methane + propane) system, J. Chem. Thermodyn., 99 (2016) 105-115.
[9] H. Quinteros-Lama, F. Llovell, Global phase behaviour in methane plus n-alkanes binary mixtures, J. Supercrit. Fluids, 111 (2016) 151-161.
[10] D. Rowland, T.J. Hughes, E.F. May, Extending the GERG-2008 equation of state: Improved departure function and interaction parameters for (methane + butane), J. Chem. Thermodyn., 97 (2016) 206-213.
[11] V. Papaioannou, F. Calado, T. Lafitte, S. Dufal, M. Sadeqzadeh, G. Jackson, C.S. Adjiman, A. Galindo, Application of the SAFT-γ Mie group contribution equation of state to fluids of relevance to the oil and gas industry, Fluid Phase Equilib., 416 (2016) 104-119.
[12] L.E. Urlic, L.J. Florusse, E.J.M. Straver, S. Degrange, C.J. Peters, Phase and interfacial tension behavior of certain model gas condensates: Measurements and modeling, Transp. Porous Media, 52 (2003) 141-157.
[13] H.H. Reamer, B.H. Sage, W.N. Lacey, Phase equilibria in hydrocarbon systems - methane-n-butane-becane system, Ind. Eng. Chem., 39 (1947) 77-82.
[14] H.H. Reamer, J.M. Fiskin, B.H. Sage, Phase equilibria in hydrocarbon systems, Ind. Eng. Chem., 41 (1949) 2871-2875.
[15] H.H. Reamer, B.H. Sage, W.N. Lacey, Phase equilibria in hydrocarbon systems. Volumetric and phase behavior of the methane-n-butane-decane system, Ind. Eng. Chem., 43 (1951) 1436-1444.
[16] H.H. Reamer, B.H. Sage, W.N. Lacey, Phase equilibria in hydrocarbon systems - methan-n-butane-decane system at 40° F, Ind. Eng. Chem., 44 (1952) 1671-1675.
[17] H.H. Reamer, V.M. Berry, B.H. Sage, Phase equilibriums in hydrocarbon systems. Volumetric behavior in the methane-propane-n-decane system, J. Chem. Eng. Data, 14 (1969) 447-454.
[18] M. Kariznovi, H. Nourozieh, J. Abedi, Experimental and thermodynamic modeling study on (vapor + liquid) equilibria and physical properties of ternary systems (methane + n-decane + n-tetradecane), Fluid Phase Equilib., 334 (2012) 30-36.
[19] M. Kariznovi, H. Nourozieh, J. Abedi, Vapor–liquid phase equilibria and physical properties measurements for ternary systems (methane + decane + hexadecane), J. Chem. Eng. Data, 57 (2012) 2535-2542.
[20] M.J. Cebola, G. Saville, W.A. Wakeham, Vapor–liquid equilibrium in the ternary system methane-n-hexane-n-tetradecane, Fluid Phase Equilib., 150–151 (1998) 703-711.
[21] J. Gregorowicz, T.W. de Loos, J. de Swaan Arons, Liquid-liquid-vapour phase equilibria in the system ethane + propane + eicosane: retrograde behaviour of the heavy liquid phase, Fluid Phase Equilib., 84 (1993) 225-250.
[22] J.J.B. Machado, T.W. de Loos, High pressure solid–fluid and vapour–liquid equilibria in model hyperbaric fluids: the system methane + tetracosane + triacontane, Fluid Phase Equilib., 228–229 (2005) 261-268.
[23] T. Yang, W.-D. Chen, G. Tian-Min, Phase behavior of an asymmetric ternary mixture in the near-critical region, Chem. Eng. Sci., 52 (1997) 259-267.
[24] V. Uribe-Vargas, A. Trejo, Vapor–liquid equilibrium of methane and methane + nitrogen and an equimolar hexane + decane mixture under isothermal conditions, Fluid Phase Equilib., 238 (2005) 95-105.
[25] S.a.T. Blanco, S. Avila, I. Velasco, E. Rauzy, S. Otín, Dew points of ternary methane+ethane+butane and quaternary methane+ethane+butane+water mixtures: measurement and correlation, Fluid Phase Equilib., 171 (2000) 233-242.

[26] J.L. Daridon, P. Xans, F. Montel, Phase boundary measurement on a methane + decane + multi-paraffins system, Fluid Phase Equilib., 117 (1996) 241-248.
[27] F. Gozalpour, A. Danesh, A.C. Todd, D.H. Tehrani, B. Tohidi, Vapour–liquid equilibrium volume and density measurements of a five-component gas condensate at 278.15–383.15 K, Fluid Phase Equilib., 206 (2003) 95-104.
[28] Ø. Mørch, K. Nasrifar, O. Bolland, E. Solbraa, A.O. Fredheim, L.H. Gjertsen, Measurement and modeling of hydrocarbon dew points for five synthetic natural gas mixtures, Fluid Phase Equilib., 239 (2006) 138-145.
[29] H. Nourozieh, M. Kariznovi, J. Abedi, Solubility measurements and saturated liquid properties of ternary systems (methane + decane + octadecane) at 295 K, J. Chem. Eng. Data, 57 (2012) 2513-2519.
[30] J. Pauly, J.A.P. Coutinho, J.-L. Daridon, High pressure phase equilibria in methane + waxy systems. 2. Methane + waxy ternary mixture, Fluid Phase Equilib., 297 (2010) 149-153.
[31] J. Pauly, J.A.P. Coutinho, J.-L. Daridon, High pressure phase equilibria in methane + waxy systems. 3. Methane + a synthetic distribution of paraffin ranging from n-C13 to n-C22, Fluid Phase Equilib., 313 (2012) 32-37.
[32] A. Shariati, C.J. Peters, M. Moshfeghian, Bubble-point pressures of some selected methane + synthetic C6+ mixtures, J. Chem. Eng. Data, 43 (1998) 280-282.
[33] A. Fenghour, J.P.M. Trusler, W.A. Wakeham, Densities and bubble points of ternary mixtures of methane, n-butane and n-hexadecane and quaternary mixtures of methane, n-butane, n-heptane and n-hexadecane, Fluid Phase Equilib., 182 (2001) 111-119.
[34] T. Regueira, G. Pantelide, W. Yan, E.H. Stenby, Density and phase equilibrium of the binary system methane + n-decane under high temperatures and pressures, Fluid Phase Equilib., 428 (2016) 48-61.
[35] G. Soave, Equilibrium constants from a modified Redlich-Kwong equation of state, Chem. Eng. Sci., 27 (1972) 1197-1203.
[36] D.-Y. Peng, D.B. Robinson, A new two-constant Equation of State, Ind. Eng. Chem. Fundam., 15 (1976) 59-64.
[37] J. Gross, G. Sadowski, Perturbed-Chain SAFT: An equation of state based on a perturbation theory for chain molecules, Ind. Eng. Chem. Res., 40 (2001) 1244-1260.
[38] G.S. Soave, An effective modification of the Benedict–Webb–Rubin equation of state, Fluid Phase Equilib., 164 (1999) 157-172.
[39] O. Kunz, W. Wagner, The GERG-2008 wide-range equation of state for natural gases and other mixtures: An expansion of GERG-2004, J. Chem. Eng. Data, 57 (2012) 3032-3091.
[40] W. Yan, F. Varzandeh, E.H. Stenby, PVT modeling of reservoir fluids using PC-SAFT EoS and Soave-BWR EoS, Fluid Phase Equilib., 386 (2015) 96-124.
[41] E.W. Lemmon, M.L. Huber, M.O. McLinden, NIST Reference Fluid Thermodynamic and Transport Properties Database (REFPROP): Version 9.1, in, 2013.
[42] E.W. Lemmon, R. Span, Short fundamental equations of state for 20 industrial fluids, J. Chem. Eng. Data, 51 (2006) 785-850.
[43] E.W. Lemmon, M.L. Huber, Thermodynamic properties of n-dodecane, Energy Fuels, 18 (2004) 960-967.
[44] N. von Solms, I.A. Kouskoumvekaki, M.L. Michelsen, G.M. Kontogeorgis, Capabilities, limitations and challenges of a simplified PC-SAFT equation of state, Fluid Phase Equilib., 241 (2006) 344-353.
[45] M. Benedict, G.B. Webb, L.C. Rubin, An empirical equation for thermodynamic properties of light hydrocarbons and their mixtures I. Methane, ethane, propane and n-butane, J. Chem. Phys., 8 (1940) 334-345.

[46] Design Institute for Physical Property Research Database DIPPR Project 801, in, Design Institute for Physical Property Research / AIChE, 2015.
[47] D. Ambrose, C. Tsonopoulos, Vapor-liquid critical properties of elements and compounds. 2. Normal alkanes, J. Chem. Eng. Data, 40 (1995) 531-546.
[48] C. Tsonopoulos, Z. Tan, The critical constants of normal alkanes from methane to polyethylene: II. Application of the Flory theory, Fluid Phase Equilib., 83 (1993) 127-138.
[49] F. Varzandeh, E.H. Stenby, W. Yan, Comparison of GERG-2008 and simpler EoS models in calculation of phase equilibrium and physical properties of natural gas related systems, Fluid Phase Equilib., 434 (2017) 21-43.

- Bubble points found for low GOR system and dew points found for C_1-C_4-C_{10}, C_1-C_4-C_{12}, and high GOR systems
- Maximum liquid fractions of 0.38, 0.31 and 0.29 were found for C_1-C_4-C_{10}, C_1-C_4-C_{12}, and high GOR systems, respectively
- PR and PC-SAFT have a better overall performance in the prediction of the experimental saturation pressures
- Liquid fractions of the low GOR mixture are predicted with an AAD lower than 8% through all models
- C_1-C_4-C_{10}, C_1-C_4-C_{12}, and high GOR liquid fractions are predicted satisfactorily at pressures up to 80 % of saturation pressure